脳FDG・アミロイドPETにおける画像再構成条件の最適化

赤松, 剛

https://doi.org/10.15017/1654738

TITLE:

Optimization of image reconstruction conditions with phantoms for brain FDG and amyloid PET imaging

Go Akamatsu[1, 2], Yasuhiko Ikari[1], Tomoyuki Nishio[1], Hiroyuki Nishida[1], Akihito Ohnishi[1], Kazuki Aita[1], Masahiro Sasaki[1], Masayuki Sasaki[2], Michio Senda[1]

1. Division of Molecular Imaging, Institute of Biomedical Research and Innovation
2. Department of Health Sciences, Graduate School of Medical Sciences, Kyushu University

Corresponding author:

Michio Senda, MD, PhD

Division of Molecular Imaging, Institute of Biomedical Research and Innovation

2-2, Minatojima-Minamimachi, Chuo-ku, Kobe 650-0047, Japan

TEL: +81-78-304-5212, FAX: +81-78-304-5201

E-mail: senda@fbri.org

First author:

Go Akamatsu, MS

Division of Molecular Imaging, Institute of Biomedical Research and Innovation

2-2, Minatojima-Minamimachi, Chuo-ku, Kobe 650-0047, Japan

TEL: +81-78-304-5212, FAX: +81-78-304-5201

Department of Health Sciences, Graduate School of Medical Sciences, Kyushu University

3-1-1, Maidashi, Higashi-ku, Fukuoka 812-8582, Japan

E-mail: akamatsu@fbri.org, golilin5@gmail.com

PhD student

The type of article: original article

The word count of the manuscript: 6088 words

*Footnotes: Optimization for Amyloid Brain PET

Conflict of interest:

Institute of Biomedical Research and Innovation carried out clinical trial of

^{18}F-florbetapir and ^{18}F-flutemetamol sponsored by AVID/Eli Lilly and GE Healthcare, respectively, with Michio Senda as principal investigator.

Abstract

Objectives: The purpose of this study was to optimize image reconstruction conditions for brain ^{18}F-FDG, ^{11}C-PiB, ^{18}F-florbetapir and ^{18}F-flutemetamol PET imaging with Discovery-690 PET/CT for diagnosis and research on Alzheimer's disease (AD) based on the standard imaging protocols and phantom test procedures and criteria published by the Japanese society of nuclear medicine (JSNM). **Methods:** A Hoffman 3D brain phantom and a cylindrical pool phantom were scanned according to the JSNM procedure, and the reconstruction conditions (iteration, subset, post-filter) were optimized so that the images satisfy the JSNM criteria regarding spatial resolution (FWHM ≤8mm) and gray/white matter contrast (%contrast ≥55%) on the Hoffman phantom and uniformity (SD of small ROIs ≤0.0249) and image noise (coefficient of variation ≤15%) on the pool phantom. Human images were acquired with ^{18}F-FDG (15-min scan starting at 30 min post injection [p.i.] of 185 MBq), ^{11}C-PiB (20-min scan starting at 50 min p.i. of 555 MBq), ^{18}F-florbetapir (10-min scan starting at 50 min p.i. of 370 MBq) and ^{18}F-flutemetamol (30-min scan starting at 90 min p.i. of 185 MBq) on 1 or 2 subjects for each tracer and reconstructed with thus determined conditions to evaluate the image quality visually. The effect of reconstruction parameters on the standardized uptake value ratio (SUVR) was also evaluated on 5 amyloid positive and 5

negative PiB images. **Results:** A sufficient image quality was obtained at an iterative update (product of iteration and subset) of 64 for ^{18}F-FDG. The same reconstruction parameters with an additional Gaussian filter of 5 mm FWHM was optimal for ^{11}C-PiB, ^{18}F-florbetapir and ^{18}F-flutemetamol to achieve the phantom criteria. Those optimal reconstruction conditions were confirmed with human images. The SUVR value was stable over a wide range of iterative updates around the optimal parameters both for positive and negative amyloid images. **Conclusions:** Optimal image reconstruction conditions were determined for brain ^{18}F-FDG and amyloid PET imaging with Discovery-690 PET/CT for diagnosis and research on AD based on the JSNM phantom criteria. This supports feasibility of the phantom criteria for standardization and harmonization of brain ^{18}F-FDG and amyloid PET for multi-center studies.

Key Words: ^{18}F-FDG; amyloid; reconstruction parameter; Alzheimer's disease; standardized uptake value ratio

Introduction

Brain PET imaging with ^{18}F-FDG and amyloid tracers is useful for early and/or differential diagnosis of Alzheimer's disease (AD) [1]. Amyloid brain PET is also used for screening and evaluation of responses to treatment in clinical trials of AD therapeutics [2]. The United States (US) Food and Drug Administration (FDA) has approved three β-amyloid agents, i.e. ^{18}F-florbetapir, ^{18}F-flutemetamol and ^{18}F-florbetaben [3–6], while ^{11}C-PiB has been universally used for research [1,7]. Those amyloid tracers in general accumulate in pathological cortical β-amyloid plaques and non-specifically in the white matter, but present various amount of brain uptake according to the tracer characteristics and injection activity [3]. The value of standardized uptake value ratio (SUVR), which is frequently used to measure of β-amyloid deposition, also depends on the tracer [3].

Physical quality of PET images such as image resolution and noise depends on the PET camera model, having various intrinsic resolution and sensitivity, as well as on the reconstruction conditions, which include reconstruction parameters and post-filter. Image quality may affect visual interpretation of the images and also influences quantified values such as 3-dimensional stereotactic surface projection (3D-SSP) statistical analysis of ^{18}F-FDG PET and SUVR of amyloid images [8]. Therefore, in

multicenter clinical studies, participating PET centers are requested to test their PET cameras with the phantoms to determine the reconstruction conditions applicable to the PET camera and to confirm the image quality obtained with the PET camera on site [8–10].

An iterative reconstruction method is generally used for image reconstruction of brain PET with ^{18}F-FDG and amyloid tracers although filtered back projection method is still used [5]. Parameters of the iterative reconstruction, including the number of iterations and subsets, and the post-filter substantially affect the image quality and might ideally be determined by a phantom experiment that imitates the amount and distribution of radioactivity in the human PET scans. Optimization of reconstruction conditions is required to obtain better image quality as well as to harmonize quantitative metrics among different PET cameras [11,12]. However, few studies evaluated the effect of the reconstruction conditions in brain PET imaging. Furthermore, dedicated PET cameras have been used in many of previous brain PET studies, and few data have been reported regarding the reconstruction conditions for new generation PET/CT cameras, which are spreading to the PET community but are oriented to whole-body oncology ^{18}F-FDG-PET and may lack consideration for brain imaging [13–15]. Optimization of reconstruction conditions for new generation PET/CT cameras should

be important to make ^{18}F-FDG and amyloid PET a universal tool because use of PET will increase in the clinical practice on AD in the future.

In the US and Japanese Alzheimer's disease neuroimaging initiative (ADNI and J-ADNI) multi-center study [8,10], the reconstruction parameters were determined based on the experiments with the Hoffman 3D brain phantom so as to achieve a certain level of image quality and resolution (<8 mm FWHM) [16,17]. The J-ADNI followed the reconstruction parameters for the camera models used in the ADNI project of US if they are used in both of them, but optimized the parameters by themselves for those PET cameras only used in J-ADNI [8,10,16]. Recently, the J-ADNI team planned another multi-center study project, which would cover more PET camera models for standardization and harmonization. To facilitate harmonization between different camera models, the Japanese Society of Nuclear Medicine (JSNM) issued "Standard PET imaging protocols and phantom test procedures and criteria" based on the J-ADNI criteria [18]. This phantom test procedure is becoming the standard of brain PET imaging method in Japan, as the Japanese regulators recommended conforming to the society guideline when they approved a synthesizing device of an amyloid PET tracer.

In this study, we determined optimal reconstruction conditions for brain ^{18}F-FDG, ^{11}C-PiB, ^{18}F-florbetapir and ^{18}F-flutemetamol PET based on the JSNM

phantom test procedures by using a Discovery-690 PET/CT. We then visually evaluated the human brain PET images acquired with ^{18}F-FDG, ^{11}C-PiB, ^{18}F-florbetapir and ^{18}F-flutemetamol and reconstructed with the conditions optimized with the phantoms. The quantitative effect of the reconstruction parameters on the SUVR of the human ^{11}C-PiB images was also evaluated.

Materials and Methods

PET/CT Scanner Specifications

A Discovery-690 PET/CT unit (GE Healthcare, Milwaukee, WI) was used for all PET imaging in this study [19]. This PET scanner comprised a total of 13,824 LYSO crystals with dimensions of 4.2×6.3×25 mm^3, covering an axial field-of-view (FOV) of 15.7 cm and a transaxial FOV of 70 cm in diameter. The PET component consists of 24 rings of detectors with 576 crystals per detector ring. The coincidence time window was 4.9 ns. The sinogram binnings for 3D acquisition were 381 radial bins and 288 projection-angle bins. The PET data were acquired in 3-dimensional (3D) mode with acceptance of ±23 planes, and reconstructed with the 3D ordered subsets expectation maximization (OSEM) algorithms. A 2D Gaussian filter and a “standard” Z-axis filter were used as a post-smoothing filter. Neither point-spread function (PSF) nor

time-of-flight (TOF) reconstruction was used in this study as they were not used in the ADNI 2 study [20]. PSF and TOF are useful for oncology whole-body FDG-PET because they improve image quality and lesion detectability. However, the utilities of PSF and TOF were not established for brain PET. Review article written by Rahmim et al. reported that PSF causes edge artifact and challenges quantitative accuracy [21]. On the other hand, Bettinardi et al. [19] reported that the effect of TOF is relatively small for brain PET because the TOF gain depends on object size [22,23]. The image matrix was 128×128 with a 2.00 mm pixel size. The display FOV was 25.6 cm. The PET image slice thickness was 3.27 mm. CT scan for attenuation correction was performed using the following parameters: 120 kV, 40 mA, 0.5-s tube rotation, and 5-mm slice collimation.

Phantom Study

Data acquisition. A Hoffman 3D brain phantom (Data Spectrum Corporation, Hillsborough, NC) and a cylindrical pool phantom (Itoi Factory Inc, Kobe, Japan) were used in the phantom study according to the JSNM phantom test procedures. The Hoffman phantom realizes the 4:1 ratio in the apparent “gray matter” to “white matter” activity concentration [24]. The cylindrical pool phantom is made of acrylic resin and

accommodates 16 cm inner diameter and 30 cm inner length. First, the Hoffman phantom was filled with an ^{18}F solution of 20 MBq at the start of emission scan and was scanned for 30 min in list-mode, together with the uniform cylindrical pool phantom containing 80 MBq of an ^{18}F solution placed 30 cm apart from the end of the Hoffman phantom on the bed out of the field to simulate body activity. Second, the cylindrical pool phantom was placed alone at the center of FOV and scanned for 30 min in list-mode starting at the activity of 40 MBq.

Data processing. Table 1 shows the JSNM standard imaging protocols and the modified protocols adopted in our study using the Discovery-690 scanner. JSNM states that the scan time is changeable according to each study protocol and performance of the PET camera and may be determined based on the phantom study [18]. In this study, we shortened the emission scan durations of ^{18}F-FDG and ^{18}F-florbetapir PET according to the sponsor of the corresponding human study written below (Table 1). Table 1 also shows the estimated whole brain uptake for each tracer [10,25–27], based on which JSNM phantom procedures were determined. The 30 min acquisition list-mode data were sorted so as to extract data of various count statistics corresponding to each tracer as shown in Table 2 so that the decay-incorporated product of activity and scan time (number of disintegration) would be equal to the human protocol. Considerations were

also given to physical decay and branching fraction of ^{11}C and ^{18}F. The difference in the activity between the human brain and phantoms would not affect the results, considering the count-rate performance of the Discovery-690 scanner. The phantom images were reconstructed using OSEM with variable number of iterations (1~16) and subsets (4~24). A Gaussian post-filter was applied having FWHM of 0~8 mm.

Image Analysis. Image quality was assessed according to the JSNM phantom test procedures to obtain four physical indicators, and the influence of reconstruction parameters was evaluated. The four physical indicators were image spatial resolution, gray-to-white contrast, uniformity, and image noise, all of which were selected as essential image quality for brain ^{18}F-FDG and amyloid PET imaging [18]. PMOD ver3.4 software (PMOD group, Switzerland) was used to analyze both visually and quantitatively to derive the four physical indicators: spatial resolution and contrast (%contrast) based on the Hoffman phantom image and uniformity ($SD_{uROImean}$) and image noise (coefficient of variation; CV) based on the uniform cylindrical phantom image.

Spatial resolution was estimated from visual similarity between the Hoffman phantom image and the digital phantom obtained from the vendor treated with a 3D Gaussian filter of various FWHMs [24].

To derive %contrast, first, the Hoffman phantom image was co-registered to the digital phantom using normalized mutual information method implemented in PMOD software. Then, the JSNM region of interest (ROI) template, which had been created to cover gray matter and white matter regions of the Hoffman phantom, were applied to the co-registered PET image [18,28]. The ROI template covered the regions characterized by frequent deposition of β-amyloid plaque in the Alzheimer pathology. The %contrast was calculated as follows:

$$\%\text{contrast} = [(GM_P/WM_P - 1) / (GM_d/WM_d - 1)] \times 100\ (\%) \quad (1)$$

where GM_P and WM_P were ROI average activity of the gray matter and white matter on the phantom PET image, and GM_d and WM_d were ROI average value of the gray matter and white matter on the digital phantom image, respectively.

For uniformity evaluation, 17 circular ROIs of 500 mm^2 (uROI) were placed on the central slice and on slices ±40 mm apart from the central slice (a total of 51 uROIs) for the pool phantom image with scan duration of 30 min. Because we want to minimize the effect of noise, phantom image of the maximum scan duration was used instead of extracted data from the list-mode acquisition. The $SD_{uROImean}$ was calculated as follows:

$$SD_{uROImean} = \sqrt{\frac{1}{n}\sum_{i=1}^{n}\left(\frac{uROI_{mean,i}}{uROI_{TOT}} - 1\right)^2} \quad (2)$$

where $uROI_{mean}$ is the mean activity of uROI (n=51) and $uROI_{TOT}$ is the average of the

51 $uROI_{mean}$.

For image noise evaluation, a circular 13-cm-diameter ROI (nROI) was placed on the center of the pool phantom image. The CV was then calculated as follows:

$$CV = SD/nROI_{mean} \times 100\ (\%) \qquad (3)$$

where SD is the standard deviation of nROI activity and $nROI_{mean}$ is the mean of nROI activity.

The measured physical indicators were compared with the JSNM image quality acceptance criteria presented below.

- Spatial resolution: 8 mm FWHM or better spatial resolution in the Hoffman 3D brain phantom
- Contrast: 55% or better %contrast in the Hoffman 3D brain phantom
- Uniformity: $SD_{uROImean} \leq 0.0249$ in the uniform cylindrical phantom, which corresponds to 95% of the $uROI_{mean}$ being distributed within 1.00±0.05 assuming normal distribution.
- Image noise: CV ≤ 15% in the uniform cylindrical phantom

Optimal reconstruction parameters and post-filters were determined that satisfied the above criteria.

Evaluation of Human Image Quality Based on Phantom Optimization

As an exemplification of the phantom optimization, image quality was visually evaluated on a few representative human brain PET images of the four tracers that had been acquired in other research projects according to the imaging protocols shown in Table 1 and were reconstructed with the conditions optimized in the present phantom study.

Profile of human images. PET images of a total of 7 subjects obtained with the Discovery-690 scanner were evaluated: 1 with ^{18}F-FDG, 2 with ^{11}C-PiB, 2 with ^{18}F-florbetapir and 2 with ^{18}F-flutemetamol. The 2 subjects for each amyloid tracer injection were composed of 1 positive and 1 negative subject. The 7 subjects had been enrolled in other clinical studies and trials that had been approved by the ethics committee or the institutional review board of our institute, and all had signed an informed consent. The ^{18}F-FDG images had been acquired on a 32-year old normal subject in an investigator-sponsored study of our own program. The ^{11}C-PiB images had been acquired on normal and AD subjects in another investigator-sponsored study. The ^{18}F-florbetapir and ^{18}F-flutemetamol images had been acquired on normal and AD subjects in the respective phase-II clinical trial of a PET diagnostic tracer sponsored by AVID/Eli Lilly and GE Healthcare, respectively. The use of those human images for the

present study was retrospective, and its results did not influence in any way the original clinical research and trials or further therapeutic decision making. The imaging protocol for each tracer is shown in Table 1. The human PET images were reconstructed with the optimal conditions determined by the present phantom study and the images were interpreted by 2 nuclear physicians regarding the quality and the presence of abnormal accumulation [29,30].

Effect of Reconstruction Parameters on Quantitative SUVR in ^{11}C-PiB Human Brain Imaging

Image Acquisition. The effect of reconstruction parameters on the quantitative SUVR measurement in ^{11}C-PiB images was evaluated on a total of 10 subjects (mean age, 69.8±9.3 y) who had undergone MRI and ^{11}C-PiB PET/CT in another study project. The original clinical study had been approved by the ethics committee, and all subjects had signed an informed consent form. The present data analysis was retrospective, and did not influence the original study or any further therapeutic decision making. The clinical diagnoses for these patients had been Alzheimer's disease (n = 1), mild cognitive impairment (MCI) (n = 5) and healthy control (n = 4). The mini mental state examination (MMSE) [31], which is 30-points neuropsychological test used extensively

in clinical and research settings to measure cognitive impairment, had been 21.0 for the AD patient, 26.2±1.60 for the MCI patients and 29.8±0.43 for the healthy control subjects (mean±SD).

The MRI data had been acquired on the 1.5 Tesla SIGNA EXCITE (GE Healthcare, Milwaukee, WI). Axial T1-weighted 3D-SPGR images had been acquired with the following parameter: TE/TR, Min/23.0 ms; slice thickness, 2.0 mm; FOV, 22.0 cm; number of slices, 80; bandwidth, 20.83 Hz; flip angle, 30°.

All patients had received an intravenous injection of 578.4±21.7 MBq (range, 543.5–624.5 MBq) of ^{11}C-PiB followed by a 3D emission scan of 20 min starting at 50 min post injection on the Discovery-690 scanner. For the present data analysis, the reconstruction parameters were varied so that the iterative updates (product of iterations and subsets) ranged from 4 to 128, and a 5mm-FWHM Gaussian post-filter was applied, whereas the original study had adopted 4 iterations, 16 subsets, and 5 mm FWHM Gaussian.

Image Analysis. Using PMOD ver3.4 software, probability maps of gray matter (GM) and white matter (WM) were calculated based on the individual 3D MR image. Then, the PET image of each subject was rigidly aligned to the MR image using the normalized mutual information method, and the stereotactic transformation between the

subject MR and the standard Montreal Neurological Institute (MNI) template was performed to spatially normalize individual PET and MR images. The volume-of-interest (VOI) template of automatic-anatomic-labeling-merged (AAL-merged) atlas defined in PMOD was transformed into the subject PET images using the inverse transformation. The mean activities in the following regions were obtained: precuneus posterior cingulate, frontal cortex, lateral temporal cortex, parietal cortex, and cerebellar cortex. The SUVR was calculated as the average of each regional activity normalized by the mean activity of the cerebellar cortex.

Results

Phantom Study

Uniformity only slightly varied depending on the reconstruction parameters and strength of the post-filter, and satisfied the JSNM criteria in all reconstruction conditions. The $uROI_{mean}$ distributed within 1.00±0.05 and $SD_{uROImean}$ was 0.0116 under the optimized reconstruction condition determined below.

The spatial resolution correlated with %contrast and strongly depended on the reconstruction parameters and the post-filter. Because the spatial resolution achieved the JSNM criteria (≤ 8mm FWHM) whenever the %contrast satisfied the criteria, the results

of the spatial resolution were presented only for the optimal reconstruction conditions as determined below.

Fig. 1AB shows the %contrast and CV as a function of the number of iterative updates (product of iterations and subsets) computed on the phantom images acquired in the condition of each tracer. The phantom images for the three amyloid tracers, but not for ^{18}F-FDG, were treated with a post-filter of 5 mm FWHM Gaussian, which was determined as described below. The %contrast increased as the number of iterative updates increased, but approached a plateau after 60 updates for all tracers. The CV, representing image noise, increased as the iterative updates increased as a trade-off between %contrast and CV, but was well below the JSNM criteria below 80 updates. Based on these results, we chose the iterative updates of 64 (4 iterations and 16 subsets) as the optimal reconstruction parameters, with which both %contrast (59.2% to 65.9%) and CV (6.5% to 10.7%) satisfied the JSNM criteria (≥55% and ≤15%, respectively) for all tracers.

Fig. 1CD shows the effect of the post-filter on the %contrast and CV at iterative updates of 64. As the strength of the filter increased, both %contrast and CV decreased. Sufficient %contrast was obtained at 6 mm or less FWHM. Sufficient CV was also obtained for the phantom image for ^{18}F-FDG without Gaussian filter. On the

other hand, acceptable CV was obtained at 4 mm or stronger post-filter for amyloid tracers including ^{11}C-PiB. Therefore, we chose 5 mm FWHM Gaussian post-filter for the three amyloid tracers, considering the balance between %contrast and CV.

In summary, sufficient image quality was obtained at iterative updates of 60 to 80 without post-smoothing in the phantom images for brain ^{18}F-FDG PET. An additional Gaussian filter of 4 to 6 mm FWHM was suitable for the phantoms images representing ^{11}C-PiB, ^{18}F-florbetapir and ^{18}F-flutemetamol for amyloid imaging. Based on these data, we determined the following parameters as the optimum condition: 4 iterations, 16 subsets without post-filter for ^{18}F-FDG and the same reconstruction with a post-filter of 5 mm FWHM Gaussian (Fig. 2). On the other hand, both of spatial resolution and $SD_{uROImean}$ were satisfied with the criteria if the images were reconstructed with the optimal conditions. The number of iterations and subsets were all the same on all tracers for practical reasons. The four physical indicators on all images met the JSNM criteria when the above optimal reconstruction conditions were used.

Clinical Study for Image Quality

Fig. 3 shows representative human brain images acquired with ^{18}F-FDG, ^{11}C-PiB, ^{18}F-florbetapir and ^{18}F-flutemetamol specified in Table 1 and reconstructed

with the conditions determined by the present phantom study. The display condition for ^{18}F-florbetapir and ^{18}F-flutemetamol images followed the guideline information by the vendor of each tracer [29,30]. All images were of sufficient image quality for diagnosis of positive or negative deposition according to the 2 nuclear physicians.

The effects of the number of iterations and subsets on the ^{11}C-PiB-PET images of a positive case are shown in Fig. 4. As the number of iterative updates increased, the image contrast increased and the image noise worsened.

Clinical Study for Quantitative Assessment

Fig. 5 shows SUVR as a function of the number of iterative update for the ^{11}C-PiB PET images of the 10 subjects. For the updates under 30, SUVR slightly increased as the iterative updates increased for the positive subjects. On the other hand, for the negative subjects, the SUVR slightly decreased as the iterative updates increased. The SUVR was almost stable in case of 50 iterative updates or higher irrespective of positive or negative deposition, although image resolution and noise were variable.

Discussion

In this study, we evaluated image quality and determined optimal image reconstruction conditions for brain ^{18}F-FDG and amyloid PET imaging with Discovery-690 PET/CT camera and demonstrated applicability of the JSNM phantom criteria to the camera model. We confirmed the quality of the human images with ^{18}F-FDG, ^{11}C-PiB, ^{18}F-florbetapir and ^{18}F-flutemetamol acquired and reconstructed with the optimized conditions. We also found that SUVR, a quantitative metric of amyloid deposition, was stable with a wide range of reconstruction parameters for human ^{11}C-PiB images if the quality of the phantom image tested under those reconstruction parameters satisfied the JSNM criteria. These results indicated applicability of the JSNM phantom criteria to optimization of reconstruction conditions for brain ^{18}F-FDG and amyloid PET imaging.

Our spatial resolution estimation method is similar to the “high frequency correction” of Joshi, et al [9] except that we use visual similarity while they used least squares, and the JSNM phantom test procedure adopts visual similarity. We think that visual similarity would be more robust to noise and that it would better deal with actual research and clinical situations, where visual image interpretation is essential. As a matter of fact, visual similarity (and least squares as well) is influenced by factors other

than resolution, such as scatter and noise. This may be one of the reasons that the estimated resolution in Fig 2 does not match the formula of the root of sum of squared FWHM's [9]. In addition, the formula assumes that the image point spread function is Gaussian, which is not exactly true in actual PET images.

The scan time for ^{18}F-FDG and ^{18}F-florbetapir was 30 min and 20 min in the JSNM standard, but was shortened to 15 min and 10 min, respectively, in the present study according to the clinical study protocols, the images of which were evaluated in the present study. The JSNM standards allow adjusting the scan time according to the clinical study protocol and depending on the intrinsic performance of the PET camera as long as the phantom data satisfy the criteria. The present results indicated that sufficient quality was obtainable with the shortened scan time using the Discovery-690 PET/CT camera. This agrees with the JSNM statement that the standards and phantom criteria may be updated in the future when old cameras are replaced by newer models having better intrinsic performance [18].

Reconstruction conditions determine the balance between image spatial resolution and noise, which are both important factors for visual quality and quantitative capability in brain ^{18}F-FDG and amyloid PET images [9]. Image noise can be suppressed at the sacrifice of deteriorating image resolution either by reducing the

iterative updates or by applying a stronger post-filter. While optimum reconstruction conditions depend on the count statistics and therefore on the tracer, we decided on the same iterative updates for the four tracers for simplicity and adjusted the noise for the three amyloid tracers using a post-filter in the present study. An alternative might have been using different iterative updates for each of the four tracers. Since ^{18}F-FDG and amyloid scans are often performed together, our simplification approach may help avoid mistakes in the PET data reconstruction.

We found that sufficient image quality was obtained at the iterative update of 60~80 with OSEM in the present study. Furthermore, image noise deteriorated but contrast only slightly increased as the iterative update increased at more than 60 updates. We decided on iteration=4 and subset=16, which is the set of parameters used by many investigators that makes the iterative updates of 64 [32,33], because smaller number of iterations and larger number of subsets make the computation faster than the other way round.

The present study also examined the effect of reconstruction conditions on the SUVR of ^{11}C-PiB images and found stability of the value over a wide range of reconstruction conditions around the optimum condition. This suggests that SUVR is a robust measure of the cortical uptake of amyloid tracer and is less sensitive to image

resolution and noise. This supports the validity of SUVR in multicenter studies, which is used for evaluation of treatment response as well as an aid to visual interpretation of positivity/negativity [5,34,35].

In multicenter studies on the brain ^{18}F-FDG and amyloid PET [2,8,36], the central PET imaging core lab usually takes charge of the image quality control and determines acquisition and reconstruction conditions for each PET camera based on the phantom tests on site [8]. However, the phantom criteria and the details of the actual acquisition and reconstruction conditions for each participating PET camera are usually not published, especially in industry-sponsored clinical trial. The ADNI and J-ADNI team has published such detailed information of their studies [16,33,37], which was of great use when JSNM committee determined the phantom criteria. In the present study that also dealt with ^{18}F-labeled PET tracers, we were able to obtain information of the acquisition time and reconstruction conditions for ^{18}F-florbetapir and ^{18}F-flutemetamol scans with the Discovery-690 PET/CT from the sponsor of the respective clinical trials. Because those multicenter studies and clinical trials provide evidence of the efficacy of the PET scans and new tracers, it is desirable for the investigators and sponsors to publish such information.

One of the limitations of this study may be the difference in the count rate, or

the activity that exists in the brain, between the phantom and the actual clinical condition. The JSNM phantom procedure ignores this point and only adjusts the decay-incorporated product of the activity and data acquisition time (number of disintegration) so that the phantom data for all tracers could be acquired in one scan. To confirm the influence of activity and acquisition time, we repeatedly scanned a pool phantom containing ^{11}C solution as it decayed and found that image noise was almost constant if the integration of activity and acquisition time is the same. Therefore, we believe that the phantom containing 40 MBq of ^{18}F and scanned for 65 sec is equivalent to that with 3 MBq of ^{11}C for 1200 sec, at least using a Discovery-690 PET/CT having a good count rate characteristic covering that range of count rates. Therefore, we judged that the present phantom study was validated for assessing the image quality of the multiple tracers.

Another limitation was simple visual evaluation of human image quality. Quantitative assessments of human image quality such as contrast and image noise were not performed because the true value of human images was unknown. In fact, the ADNI quality control core evaluated not quantitatively but the number of coincidence events, artifact and header description for human image quality [8]. More rigorous methods such as receiver-operating-characteristic (ROC) analysis may be suitable for human

image quality evaluation.

Conclusions

We optimized image reconstruction conditions for brain ^{18}F-FDG, ^{11}C-PiB, ^{18}F-florbetapir and ^{18}F-flutemetamol PET imaging based on the JSNM phantom test procedures and criteria. With the optimal reconstruction conditions determined in this way, sufficient image quality was obtained on the respective human PET images and stable SUVR was obtained as a quantitative metric of amyloid deposition. This supports the feasibility of the phantom criteria for standardization and harmonization of brain ^{18}F-FDG and amyloid PET imaging for multi-center studies.

References

1. Ng S, Villemagne VL, Berlangieri S, Lee ST, Cherk M, Gong SJ, et al. Visual assessment versus quantitative assessment of 11C-PIB PET and 18F-FDG PET for detection of Alzheimer's disease. J Nucl Med. 2007;48:547–52.

2. Doody RS, Thomas RG, Farlow M, Iwatsubo T, Vellas B, Joffe S, et al. Phase 3 trials of solanezumab for mild-to-moderate Alzheimer's disease. N Engl J Med. 2014;370:311–21.

3. Rowe CC, Villemagne VL. Brain Amyloid Imaging. J Nucl Med. 2011;52:1733–40.

4. Wong DF, Rosenberg PB, Zhou Y, Kumar A, Raymont V, Ravert HT, et al. In vivo imaging of amyloid deposition in Alzheimer disease using the radioligand 18F-AV-45 (flobetapir [corrected] F 18). J Nucl Med. 2010;51:913–20.

5. Vandenberghe R, Van Laere K, Ivanoiu A, Salmon E, Bastin C, Triau E, et al. 18F-flutemetamol amyloid imaging in Alzheimer disease and mild cognitive impairment: a phase 2 trial. Ann Neurol. 2010;68:319–29.

6. Villemagne VL, Ong K, Mulligan RS, Holl G, Pejoska S, Jones G, et al. Amyloid imaging with (18)F-florbetaben in Alzheimer disease and other dementias. J Nucl Med. 2011;52:1210–7.

7. Lowe VJ, Kemp BJ, Jack CR Jr, Senjem M, Weigand S, Shiung M, et al. Comparison of 18F-FDG and PiB PET in cognitive impairment. J Nucl Med. 2009;50:878–86.

8. Jagust WJ, Bandy D, Chen K, Foster NL, Landau SM, Mathis CA, et al. The Alzheimer's Disease Neuroimaging Initiative positron emission tomography core. Alzheimers. Dement. 2010;6:221–9.

9. Joshi A, Koeppe RA, Fessler JA. Reducing between scanner differences in multi-center PET studies. Neuroimage. 2009;46:154–9.

10. Iwatsubo T. Japanese Alzheimer's Disease Neuroimaging Initiative: present status and future. Alzheimers Dement. 2010;6:297–9.

11. Akamatsu G, Ishikawa K, Mitsumoto K, Taniguchi T, Ohya N, Baba S, et al. Improvement in PET/CT image quality with a combination of point-spread function and time-of-flight in relation to reconstruction parameters. J Nucl Med. 2012;53:1716–22.

12. Lasnon C, Desmonts C, Quak E, Gervais R, Do P, Dubos-Arvis C, et al. Harmonizing SUVs in multicentre trials when using different generation PET systems: prospective validation in non-small cell lung cancer patients. Eur J Nucl Med Mol Imaging. 2013;40:985–96.

13. van Berckel BN, Ossenkoppele R, Tolboom N, Yaqub M, Foster-Dingley JC, Windhorst AD, et al. Longitudinal amyloid imaging using 11C-PiB: methodologic considerations. J Nucl Med. 2013;54:1570–6.

14. Kemppainen NM, Scheinin NM, Koivunen J, Johansson J, Toivonen JT, Någren K, et al. Five-year follow-up of 11C-PIB uptake in Alzheimer's disease and MCI. Eur J Nucl Med Mol Imaging. 2014;41:283–9.

15. Leinonen V, Rinne JO, Virtanen KA, Eskola O, Rummukainen J, Huttunen J, et al. Positron emission tomography with [18F]flutemetamol and [11C]PiB for in vivo detection of cerebral cortical amyloid in normal pressure hydrocephalus patients. Eur J Neurol. 2013;20:1043–52.

16. Ikari Y, Nishio T, Makishi Y, Miya Y, Ito K, Koeppe RA, et al. Head motion evaluation and correction for PET scans with 18F-FDG in the Japanese Alzheimer's disease neuroimaging initiative (J-ADNI) multi-center study. Ann Nucl Med. 2012;26:535–44.

17. Landau SM, Breault C, Joshi AD, Pontecorvo M, Mathis CA, Jagust WJ, et al. Amyloid-β imaging with Pittsburgh compound B and florbetapir: comparing radiotracers and quantification methods. J Nucl Med. 2013;54:70–7.

18. Standard PET imaging protocols and phantom test procedures and criteria: executive summary. Japanese Society of Nuclear Medicine website. http://www.jsnm.org/system/files/StandardPETProtocolPhantom20141225.pdf. Accessed May 29, 2015.

19. Bettinardi V, Presotto L, Rapisarda E, Picchio M, Gianolli L, Gilardi MC. Physical performance of the new hybrid PET/CT Discovery-690. Med Phys. 2011;38:5394–411.

20. ADNI 2 PET Technical Procedures Manual: Florbetapir. ADNI website. http://www.adni-info.org/scientists/doc/ADNI2_PET%20Tech_Manual-Version_4_2014Oct27_CLEAN.pdf. Accessed Jul 19.

21. Rahmim A, Qi J, Sossi V. Resolution modeling in PET imaging: theory, practice, benefits, and pitfalls. Med Phys. 2013;40:064301.

22. Surti S. Update on time-of-flight PET imaging. J Nucl Med. 2015;56:98–105.

23. Conti M. Focus on time-of-flight PET: the benefits of improved time resolution. Eur J Nucl Med Mol Imaging. 2011;38:1147–57.

24. Hoffman EJ, Cutler PD, Guerrero TM, Digby WM, Mazziotta JC. Assessment of accuracy of PET utilizing a 3-D phantom to simulate the activity distribution of [18F]fluorodeoxyglucose uptake in the human brain. J Cereb Blood Flow Metab. 1991;11:A17–25.

25. Hays MT, Segall GM. A mathematical model for the distribution of fluorodeoxyglucose in humans. J Nucl Med. 1999;40:1358–66.

26. Lin KJ, Hsu WC, Hsiao IT, Wey SP, Jin LW, Skovronsky D, et al. Whole-body biodistribution and brain PET imaging with [18F]AV-45, a novel amyloid imaging agent--a pilot study. Nucl Med Biol. 2010;37:497–508.

27. Nelissen N, Van Laere K, Thurfjell L, Owenius R, Vandenbulcke M, Koole M, et al. Phase 1 study of the Pittsburgh compound B derivative 18F-flutemetamol in healthy volunteers and patients with probable Alzheimer disease. J Nucl Med. 2009;50:1251–9.

28. Phantom test procedures and criteria [in Japanese]. Japanese Society of Nuclear Medicine website. http://www.jsnm.org/system/files/DementiaPhantomTest20150223.pdf. Accessed May 29, 2015.

29. Amyvid full prescribing information. U.S. Food and Drug Administration website. http://www.accessdata.fda.gov/drugsatfda_docs/label/2012/202008s000lbl.pdf. Accessed May 29, 2015.

30. Vizamyl full prescribing information. U.S. Food and Drug Administration website. http://www.accessdata.fda.gov/drugsatfda_docs/label/2013/203137s000lbl.pdf. Accessed May 29, 2015.

31. Folstein MF, Folstein SE, McHugh PR. "Mini-mental state". A practical method for grading the cognitive state of patients for the clinician. J Psychiatr Res. 1975;12:189–98.

32. Imabayashi E, Matsuda H, Tabira T, Arima K, Araki N, Ishii K, et al. Comparison between brain CT and MRI for voxel-based morphometry of Alzheimer's disease. Brain Behav. 2013;3:487–93.

33. Alzheimer's Disease Neuroimaging Initiative PET Technical Procedures Manual. ADNI website. http://www.adni-info.org/scientists/doc/PET-Tech_Procedures_Manual_v9.5.pdf. Accessed May 29, 2015.

34. Tiepolt S, Barthel H, Butzke D, Hesse S, Patt M, Gertz HJ, et al. Influence of scan duration on the accuracy of β-amyloid PET with florbetaben in patients with Alzheimer's disease and healthy volunteers. Eur J Nucl Med Mol Imaging. 2013;40:238–44.

35. Nemmi F, Saint-Aubert L, Adel D, Salabert AS, Pariente J, Barbeau EJ, et al. Insight on AV-45 binding in white and grey matter from histogram analysis: a study on early Alzheimer's disease patients and healthy subjects. Eur J Nucl Med Mol Imaging. 2014;41:1408–18.

36. Nordberg A, Carter SF, Rinne J, Drzezga A, Brooks DJ, Vandenberghe R, et al. A European multicentre PET study of fibrillar amyloid in Alzheimer's disease. Eur J Nucl Med Mol Imaging. 2013;40:104–14.

37. J-ADNI PET QC method [in Japanese]. J-ADNI website. http://bidb.biosciencedbc.jp/files/download/J-ADNI_PETQC_Ver1.1.pdf. Accessed May 29, 2015.

TABLE 1

Human imaging protocols for this study and JSNM standards, and estimated brain activity at the start of scan.

Radiotracer	Injection activity	Accumulation time	Scan time*	Estimated brain activity at the start of scan
^{18}F-FDG	185MBq	30min	15min (30min)	20MBq
^{11}C-PiB	555MBq	50min	20min (20min)	3MBq
^{18}F-florbetapir	370MBq	50min	10min (20min)	12MBq
^{18}F-flutemetamol	185MBq	90min	30min (30min)	3MBq

*JSNM standard scan times are noted in parenthesis.

TABLE 2

Corresponding scan duration to be extracted from the list-mode phantom data for each tracer

Radiotracer	Corresponding phantom scan duration*	
	Hoffman phantom containing 20 MBq of ^{18}F	**Pool phantom containing 40 MBq of ^{18}F**
^{18}F-FDG	900sec (1800sec)	440sec (855~865sec)
^{11}C-PiB	135sec (125~135sec)	65sec (60~70sec)
^{18}F-florbetapir	355sec (700~710sec)	175sec (340~350sec)
^{18}F-flutemetamol	255sec (245~255sec)	125sec (120~130sec)

*JSNM standard phantom scan durations are noted in parenthesis.

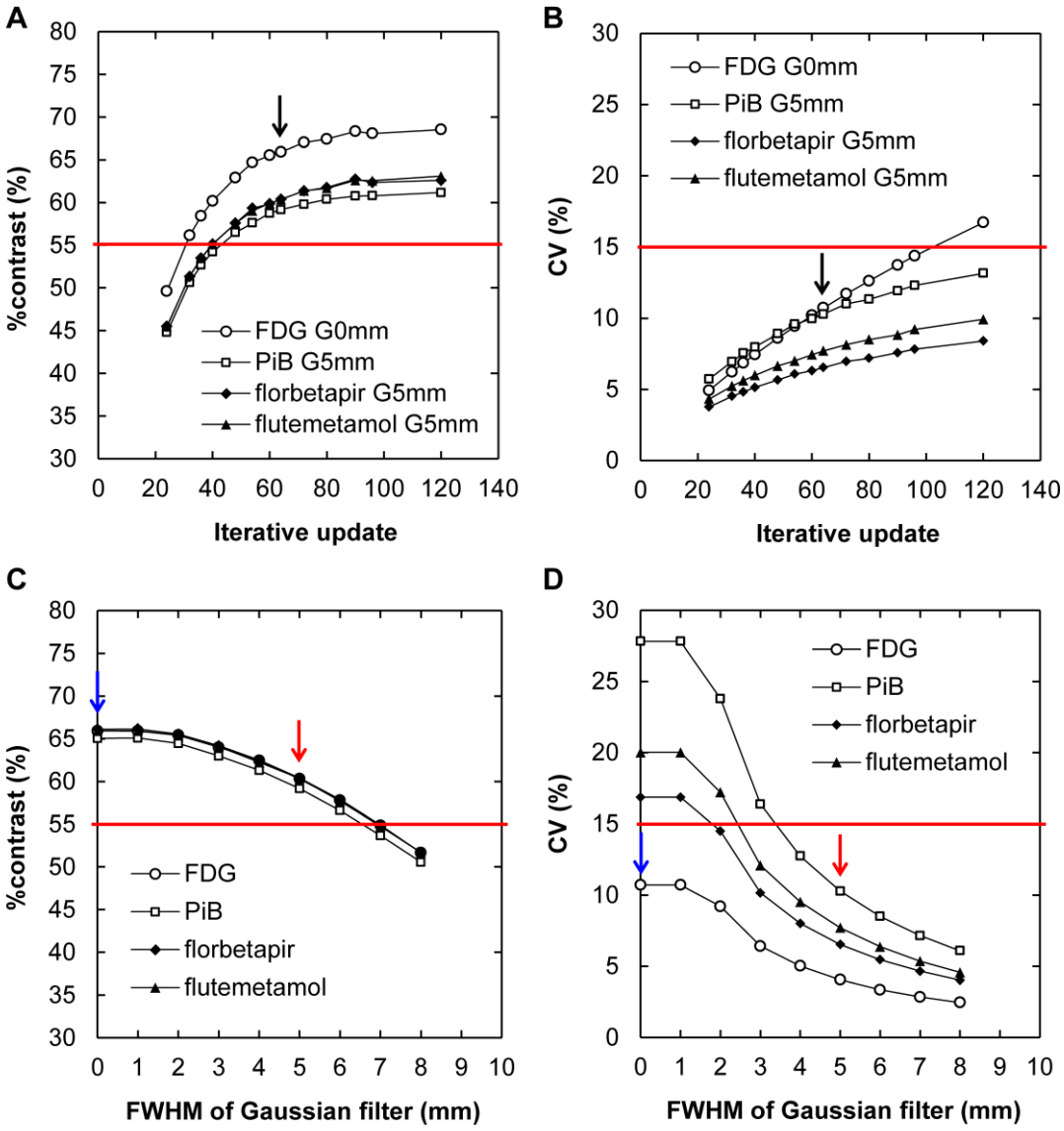

FIGURE 1. The %contrast (A,C) and coefficient of variation (CV=SD/mean) (B,D) as a function of the number of iterative updates in the OSEM reconstruction (A,B) and strength (FWHM) of the post-filter (C,D) measured on the phantom images acquired in the condition of each tracer. Arrows indicate the optimum values of the variables (64 updates and 5 mm FWHM filter) that were determined based on the data. No post-filter was applied to the images of ^{18}F-FDG condition while a post-filter of 5 mm FWHM was applied to the images of the three amyloid tracers.

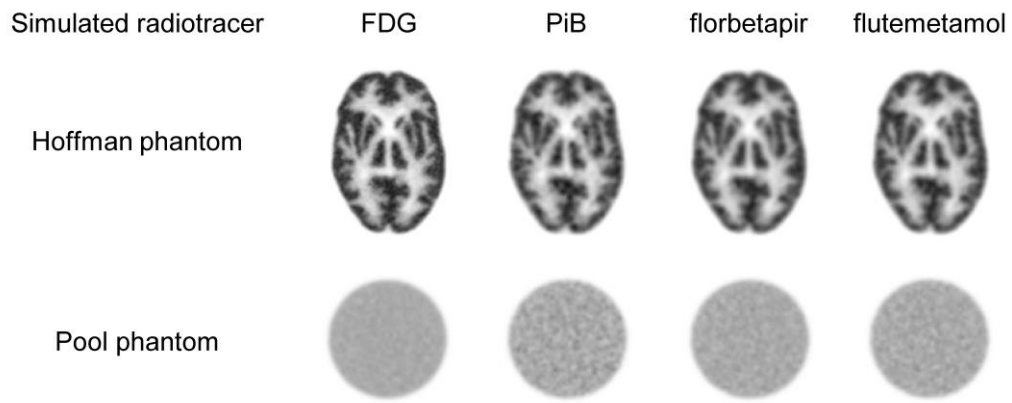

Simulated radiotracer	FDG	PiB	florbetapir	flutemetamol
Hoffman phantom				
Pool phantom				
Iteration / Subset	4 / 16	4 / 16	4 / 16	4 / 16
Gaussian filter (FWHM)	none	5mm	5mm	5mm
%contrast (%)	65.9	59.2	60.4	60.4
CV (%)	10.7	10.3	6.5	7.7
Spatial resolution	5mm	6mm	6mm	6mm
$SD_{uROImean}$		0.0116		

FIGURE 2. The PET images of both Hoffman brain phantom and the pool phantom obtained acquired in the condition of ^{18}F-FDG, ^{11}C-PiB, ^{18}F-florbetapir and ^{18}F-flutemetamol PET scan described in Table 1 and reconstructed and post-filtered with the parameters determined in the present study as they would satisfy the JSNM phantom image criteria. Based on the phantom data of the present study, phantom images were reconstructed with 4 iterations and 16 subsets without post-smoothing for ^{18}F-FDG condition. An additional Gaussian filter of 5 mm FWHM was applied to the three amyloid conditions. The criteria of %contrast (≥55%), CV (≤15%), spatial resolution (≤8mm), and $SD_{uROImean}$ (≤0.0249) were satisfied by all images.

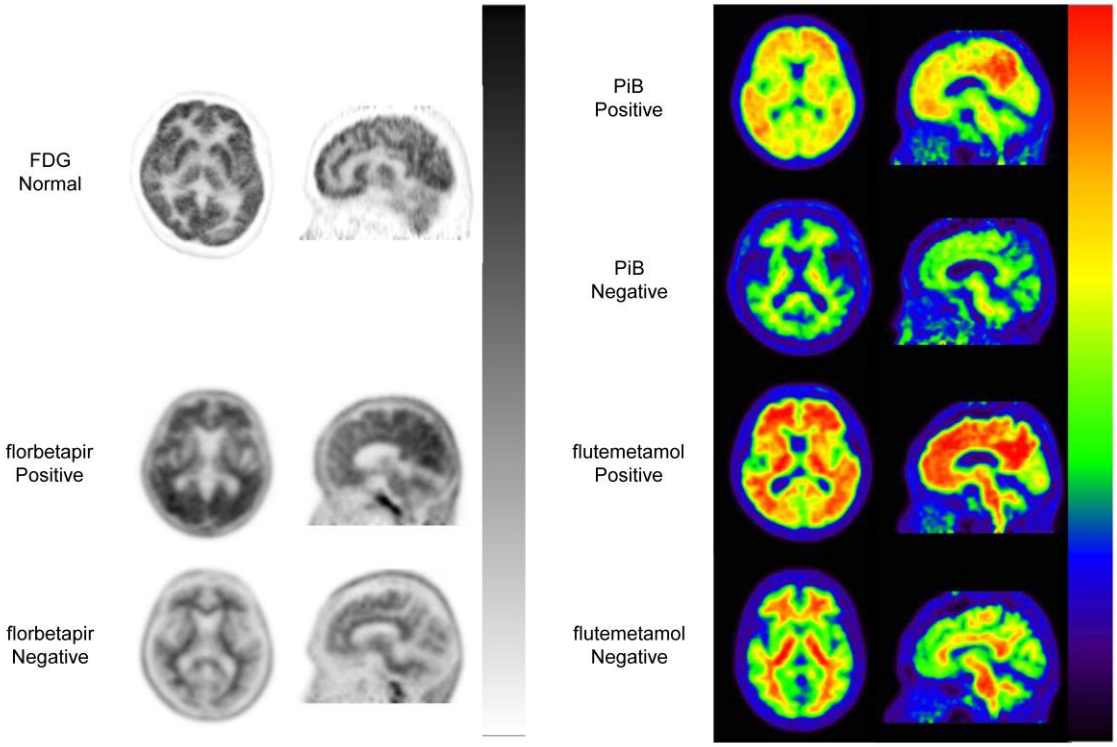

FIGURE 3. Representative human ^{18}F-FDG, ^{11}C-PiB, ^{18}F-florbetapir and ^{18}F-flutemetamol PET images acquired in the specific conditions defined in Table 1 and reconstructed with respective optimal conditions determined in the present phantom study. Sufficient image quality was obtained for all images visually.

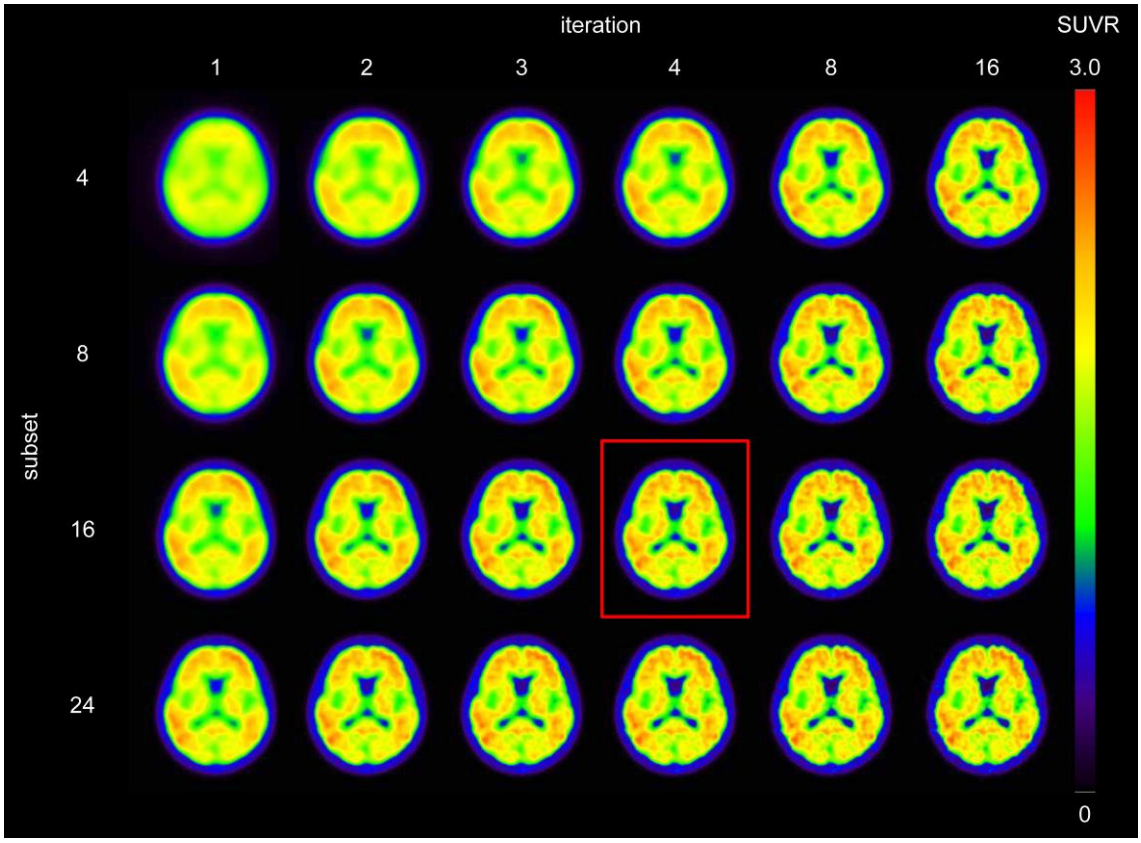

FIGURE 4. ^{11}C-PiB PET image of an amyloid-positive subject reconstructed with various iterations and subsets and filtered with 5 mm FWHM Gaussian. As the number of iterative updates (product of iterations and subsets) increased, the image contrast increased but the image noise also increased. Red frame indicates the image reconstructed with the optimal parameters determined by the phantom study.

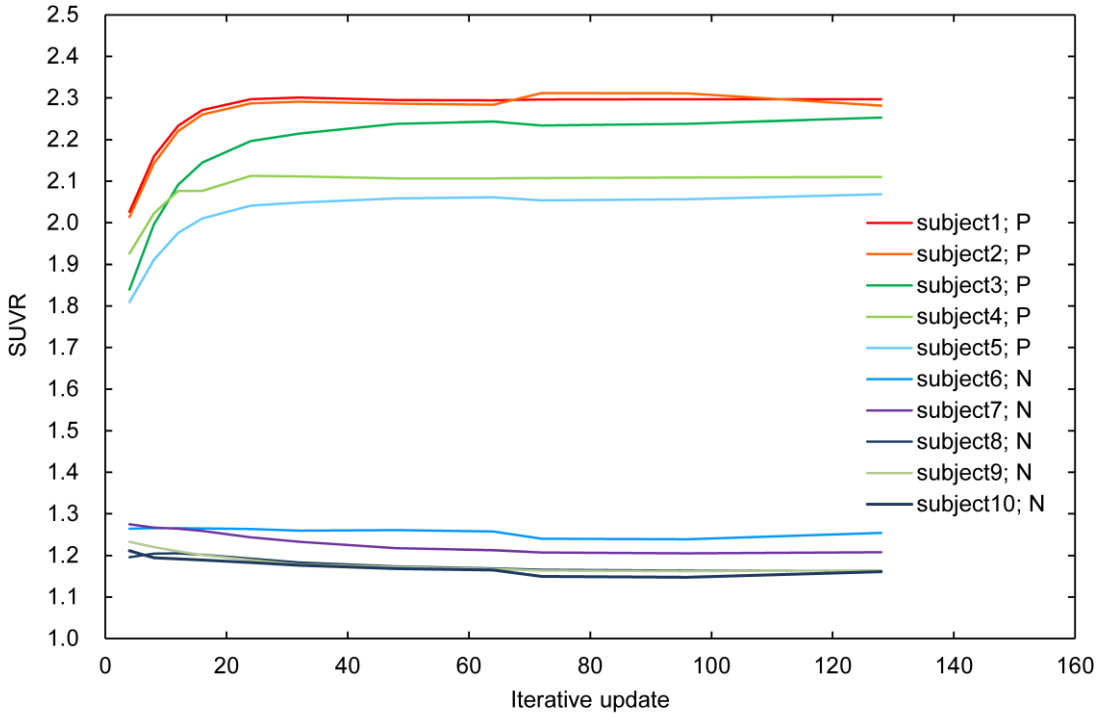

FIGURE 5. The SUVR measured on the ^{11}C-PiB PET images of the 10 subjects as a function of the number of iterative updates in the reconstruction process. The SUVR was almost constant above the iterative updates of 60 both for positive (P) and negative (N) deposition images.